# MULTIMODE Calculations of Vibrational Spectroscopy and 1d Interconformer Tunneling Dynamics in Glycine Using a Full-dimensional Potential Energy Surface

Chen Qu,[†] Paul L. Houston,[*,‡] Riccardo Conte,[*,¶] Apurba Nandi,[§] and Joel M. Bowman[*,§]

[†]*Department of Chemistry & Biochemistry, University of Maryland, College Park, Maryland 20742, U.S.A.*

[‡]*Department of Chemistry and Chemical Biology, Cornell University, Ithaca, New York 14853, U.S.A. and Department of Chemistry and Biochemistry, Georgia Institute of Technology, Atlanta, Georgia 30332, U.S.A*

[¶]*Dipartimento di Chimica, Università degli Studi di Milano, via Golgi 19, 20133 Milano, Italy*

[§]*Department of Chemistry and Cherry L. Emerson Center for Scientific Computation, Emory University, Atlanta, Georgia 30322, U.S.A.*

E-mail: plh2@cornell.edu; riccardo.conte1@unimi.it; jmbowma@emory.edu

**Abstract**

A full-dimensional, permutationally invariant polynomial potential energy surface for glycine recently reported (R. Conte et al., *J. Chem. Phys.* **2020**, *153*, 244301) is used with the code MULTIMODE to determine the IR absorption spectra for Conformers I and II using a new separable dipole moment function. The calculated spectra agree well with the experimental ones. The full-dimensional nature of the potential allows us also to examine dynamical results, such as tunneling rates. Remarkably, using a one-dimensional path based on the potential energy surface to estimate the tunneling rate from Conformer VI to Conformer I, good agreement is found with the recent experimental measurement. Finally a brief comparison of our potential energy surface with a recently reported sGDML one is made.

# Introduction

Glycine is the smallest among amino acids, being characterized by a side chain made of a single hydrogen atom. This fact has the unique consequence (for amino acids) that the $\alpha$-carbon of glycine is not chiral. Notwithstanding the simplicity of this amino acid, the electronic ground state potential energy surface (PES) of glycine has required intense investigation, and the quest for its conformers has revealed the very elusive nature of some of them.[1]

We recently reported a permutationally invariant polynomial (PIP) PES at DFT/B3LYP/aug-cc-pVDZ level of theory.[2] This PES describes the 8 low-lying conformers. Their structures were in agreement with previous calculations both by Császár,[3] whose pioneering study predicted 8 conformers but focused only on two, and by recent CCSD(T) calculations by Czakó and co-workers.[4] In addition, we performed a study of the zero-point energy of glycine by means of diffusion Monte Carlo (DMC) and semiclassical initial value representation (SCIVR) molecular dynamics. The two approaches led to results in excellent agreement with one another, allowing us to conclude that the 8 conformers could be grouped into 4

pairs of separated asymmetric double wells instead of 8 distinct conformers.

It is also worth noting that glycine has been examined recently and critically for PES fitting using a variety of machine-learning approaches.[5] (That work appeared at about the same time as our PES[2] and was evidently unaware of it.) The focus was on the flexibiliy of the glycine, as illustrated by two conformers, I and III. A sGDML PES was reported and judged to be the significantly better at describing the motion between these two conformers than the so-called Behler-Parinello NN approach[6] as well as the SchNet[7] and Gaussian Approximation Potentials (GAP).[8] Thus, it appears the glycine is also becoming a testing ground for high-dimensional PES fitting. We will examine this aspect briefly in this paper where we make a first comparison of our PIP PES with the sGDML one.

Reports on glycine in the literature have been often accompanied by a theoretical spectroscopic study of the identified isomers. This is the case of the harmonic frequency investigations by Császár[3] and later by Stepanian and Adamowicz, who validated the assignment of IR spectra for three of the conformers.[9] A major step forward in the theoretical description of glycine has been taken by introducing anharmonicity in the calculations. Gerber et al. employed vibrational self-consistent field (VSCF) theory to investigate the global minimum conformer, commonly denoted as conformer I (Conf I). They obtained results in agreement to within 40 $cm^{-1}$ with the experimental data.[10]

Conformer I as the lowest energy conformer has also attracted other studies based on very different approaches. They include models, variational, perturbative, and dynamical methods. For instance, the group of Fernandez-Clavero employed a variational procedure on a model Hamiltonian to study the low frequency modes of Conformer I.[11] Their conclusion was that a 4-dimensional Hamiltonian at least was necessary. Hobza improved investigation of the same conformer by means of second-order vibrational perturbation theory (VPT2),[12] and later Barone and co-workers developed a generalized version of it (GVPT2) to study the four energetically lowest-lying conformers.[13] Finally, results at the quantum mechanical level in excellent agreement with the GVPT2 ones were found by the Ceotto group by means

of SCIVR.[14]

Apart from estimating the anharmonic frequencies of vibration, some studies have also attempted to describe the intensities of the IR spectrum beyond the harmonic approximation. Of particular note are the reports by the Barone (VPT2, DVBP2),[13,15,16] and Ceotto (SCIVR) groups.[17]

Experimental data on the spectra are more difficult to come by, primarily because glycine is a solid at room temperature and decomposes at its melting point. Nonetheless, the vibrational and rotational spectra of glycine have long been subjects of keen investigation. Experimental studies of the rotational spectrum in the millimeter-wave region have been motivated by the 2003 report that glycine spectral lines were observed from interstellar sources,[18] but these observations were not reproduced by several other investigators.[19–21] It now appears that the presence or absence of glycine in the interstellar medium is currently unresolved and that the previous positive identification was likely in error.

The vibrational spectrum has been studied using matrix isolation spectroscopy,[9,22–25] helium droplets,[25] FTIR in liquids and solids,[26,27] and molecular beam jet cooling.[28,29] The most comprehensive results have come from matrix isolation.[9] A disadvantage of the matrix method is that the peak positions are influenced by the rare gas used as to isolate the glycine molecules, but advantages include the sharp peaks afforded by low temperatures and the possibility of identifying different conformers by the use of mid-infrared excitation of conformer overtones or ultraviolet excitation of conformer ground states, either of which can result in selective conformational changes.[22–24] The jet cooling technique has provided an excellent Raman spectra of glycine in the 180–500 $cm^{-1}$ region.[28,29]

The current investigation was motivated primarily by kinetic questions. Secondarily, we hoped to contribute to spectroscopic questions involving the coupling between different basis vibrational states and the spectra of metastable conformers. The kinetic questions are best addressed by having a global surface that accurately depicts the energetics of the stable and metastable conformers as well as the saddle points between them. The spectroscopic

questions are addressed here by determining the interaction between basis states. In the approach used by MULTIMODE[30–32] (MM) the basis states are identified with self-consistent field vibrational wavefunctions based on product harmonic oscillator wavefunctions.[30] The couplings, or configuration interactions (CI), between them, give rise both to shifts in the energy of the mixed CI states and to alterations of the intensities of the dipole allowed transitions. Although a global surface will be less spectroscopically accurate than determining the vibrational properties of a single geometry, only a global surface can address the interesting kinetic aspects of a molecule.

In this paper we address spectroscopic questions such as the vibrational transitions both from the global minimum, Conformer I, of glycine and from Conformer II. We also address kinetic questions such as the tunneling rate between Conformer VI and Conformer I.[23]

# Methods

## Potential Energy Surface

The glycine potential energy surface used here has been described previously.[2] Briefly, it is derived from a data set of energies at approximately 70,000 geometries calculated using density functional theory (B3LYP) with Dunning's aug-cc-pVDZ basis set. The fit is to 20,000 energies and their associated gradients as well as to 50,000 additional energies using a permutationally invariant polynomial basis in 45 Morse variables with maximum polynomial order of four. Investigation of the surface located eight conformers of glycine as well as 15 saddle points connecting them. The harmonic frequencies calculated for the global minimum on the surface (Conformer I) were found to agree well with those of the direct-DFT optimized structure, with a mean absolute error of 4.3 $cm^{-1}$.

## MULTIMODE Calculations

First, we present a brief recap of the VSCF[30,33] and VSCF/VCI scheme[34] in MULTIMODE.[31,32,35] The Hamiltonian (for non-linear molecules) used is the exact Watson Hamiltonian,[36] in mass-scaled normal coordinates, $\boldsymbol{Q}$. This Hamiltonian is given by

$$\hat{H} = \frac{1}{2}\sum_{\alpha\beta}(\hat{J}_\alpha - \hat{\pi}_\alpha)\mu_{\alpha\beta}(\hat{J}_\beta - \hat{\pi}_\beta) - \frac{1}{2}\sum_{k}^{F}\frac{\partial^2}{\partial Q_k^2} - \frac{1}{8}\sum_{\alpha}\mu_{\alpha\alpha} + V(\boldsymbol{Q}), \tag{1}$$

where $\alpha(\beta)$ represent the $x, y, z$ coordinates, $\hat{J}_\alpha$ and $\hat{\pi_\alpha}$ are the components of the total and vibrational angular momenta respectively, $\mu_{\alpha\beta}$ is the inverse of effective moment of inertia, and $V(\boldsymbol{Q})$ is the potential. The number of normal modes is denoted by $F$, and for non-linear molecules $F$ equals $3N-6$. In many applications of this Hamiltonian in the literature, the vibrational angular momentum terms are neglected. This approximate Hamiltonian cannot lead to exact results. We do not neglect these terms in the MULTIMODE software.

For general applications using the VSCF/VCI scheme, there are two major bottlenecks. One is the numerical evaluation of matrix elements and the second is the size of the H-matrix. Both naively have exponential dependence on the number of normal coordinates.

As an effective approach to deal with exponential scaling of matrix elements we represent the potential is the hierarchical $n$-mode representation ($n$MR) of the potential.[31] In normal coordinates, this representation is given by

$$\begin{aligned} V(Q_1, Q_2, \cdots, Q_F) = \sum_i V_i^{(1)}(Q_i) + \sum_{i,j} V_{ij}^{(2)}(Q_i, Q_j) + \\ \sum_{i,j,k} V_{ijk}^{(3)}(Q_i, Q_j, Q_k) + \sum_{i,j,k,l} V_{ijkl}^{(4)}(Q_i, Q_j, Q_k, Q_l) + \cdots, \end{aligned} \tag{2}$$

where $V_i^{(1)}(Q_i)$ is the one-mode potential, i.e., the 1D cut through the full-dimensional PES in each mode, one-by-one, $V_{ij}^{(2)}(Q_i, Q_j)$ is the intrinsic 2-mode potential among all pairs of modes, etc. Here, intrinsic means that the any $n$-mode term is zero if any of the arguments is zero. Also, each term in the representation is in principle of infinite order in the sense of

a Taylor series expansion. So for example, $V^{(1)}(Q)$ might look like a full Morse potential.

This representation has been used for nearly twenty years by a number of research groups; a sample of these are refs. 31,32,35,37–40. It continues to be actively used in a variety of applications and theoretical developments.[41–46] In MULTIMODE the maximum value of $n$ is 6. However, from numerous tests it appears that a 4MR typically gives energies that are converged to within roughly 1–5 $cm^{-1}$.[47–49] Thus we generally use 4MR with an existing full-dimensional PES and this is also done here.

The second major bottleneck to all VCI calculations is the size of the H-matrix, which as noted already can scale exponentially with the number of vibrational modes. There are many strategies to deal with this. Basically, they all limit the size of the excitation space, with many schemes taken from electronic structure theory. For example, the excitation space can be limited by using the hierarchical scheme of single, double, triple, etc. excitations. MULTIMODE uses this among other schemes and can consider up to quintuple excitations. A major difference with electronic structure theory is that the nuclear interactions go beyond 2-body. This is immediately clear from the $n$-mode representation. Thus, MULTIMODE tailors the excitation scheme for each term in this representation. Other schemes to prune the CI basis have been suggested and the reader is referred to reviews[39,41,47,50–55] for more details.

We note that the above basic VSCF/VCI scheme with the $n$-mode representation has been implemented in Molpro by Rauhut and co-workers with the option to obtain the electronic energies directly on $n$-mode grids, with $n$ up to 4 or from an existing potential.[56] Of course numerous enhancements and modifications to the basic scheme can be found there.

Finally, some comments on the limitations of rectilinear normal modes and thus the Watson Hamiltonian are in order, especially for glycine, which has low energy torsional modes. These are not expected to be accurately described especially for excited states which will exhibit large amplitude curvilinear motion. We typically either include these modes, albeit with just a small number of basis functions, or drop then from the calculation. Both

of these strategies are done here. With respect to large amplitude curvilinear motion or torsional modes, we do note that the reaction path version of MULTIMODE[57] is able to describe these. However, since such motion is not the focus of the present work we do not use this version, as it is also more computationally demanding than the version we adopt here. Thus, the spectra we present are more reliable quantitatively in the high-frequency region than in the low-frequency region.

## Details for Glycine Calculations

Calculations were performed using Version 5.1.4. of MULTIMODE.[30–32] The calculations used a four-mode representation of the potential in mass-scaled normal coordinates and a three-mode representation of the effective inverse moment of inertia for the vibrational angular momentum terms in the exact Watson Hamiltonian.[36] The formalism is based on CI from the virtual space of the ground vibrational state VSCF Hamiltonian. We explored reduced mode models as well as a full, 24-mode model. With a 9-mode model with CI blocks of size 7869 and 5064 for the $A'$ and $A''$ symmetries, we calculated 578 and 474 CI vibrational levels of these symmetries up to the energy of 5000 cm$^{-1}$. The model gave encouraging results for intensities, but several levels were significantly shifted from the experimental results. A 10-mode model was not much of an improvement. The full, 24-mode model was deemed to be the best. It had CI blocks of size 33,821 and 32,190, and we calculated 3180 and 3098 CI vibrational levels up to the energy of 3700 cm$^{-1}$.

For IR calculations a dipole moment surface is needed. The dipole-moment surface of glycine is approximated by a separable form, which in normal coordinates is given by

$$\boldsymbol{\mu}(Q_1, \ldots, Q_{24}) = \boldsymbol{\mu_e} + \sum_{i=1}^{24} \Delta\boldsymbol{\mu}_i(Q_i), \tag{3}$$

where $\boldsymbol{\mu}_e$ is the dipole moment of glycine at the equilibrium configuration, and $\Delta\boldsymbol{\mu}_i(Q_i)$ is the change of dipole caused by the change in the $i$th normal mode, obtained by a 4th-order

polynomial fit to 10 points on the 1d DFT (B3LYP/aug-cc-pVDZ) dipole cut along this mode. Note that this expansion was calculated separately for Conformer I and Conformer II.

The output from MM provided the energies of the CI states, the mixing coefficient corresponding to each basis state, and the intensity of the dipole transition between the zero-point level and each CI state. The corresponding spectrum was constructed using the CI energies and transition dipole intensities and then simulated using Gaussian peaks with full width at half maximum (FWHM) of 5 $cm^{-1}$.

## Tunneling Calculations

Because tunneling is so sensitive to the length of the tunneling path and shape of the potential above it, comparison of experimental results for the half-life with calculated estimates of tunneling provide an excellent test of a potential energy surface. Good estimates can usually not be obtained without a multidimensional PES. We have performed estimates of the tunneling rate to compare with experiment.[22] The path chosen using the PES will be discussed in a later section. Although multi-mode tunneling would provide a more accurate tunneling rate, our strategy for a simple estimate is to find the potential energy along the 1d tunneling path, letting all other coordinates relax to their minimum energy, and then to use a standard one-dimensional integral to determine the tunneling rate. The equations and method have been discussed previously.[58] Briefly, the tunneling rate constant between two conformers is given by

$$k(E) = \frac{\omega}{2\pi} exp(-2\theta), \tag{4}$$

where $\omega$ is twice the zero-point energy (ZPE) of the starting conformer,

$$\theta = \frac{1}{\hbar} \int_a^b dQ \sqrt{2[V(Q) - E]}, \tag{5}$$

and where $a$ and $b$ are the starting and ending points on the tunneling path. $V$ is the potential energy along the path and $E$ is the potential energy of the starting conformer, taken to be its ZPE for this calculation. The ZPE is calculated using the potential $V$ by means of a discrete variable representation (DVR) solution for the energy levels of the starting conformer, as described by Colbert and Miller.[59]

# Results and Discussion

## Potential Energy Surface and MULTIMODE Frequencies

Tables 1 and 2 show the results of previous calculations by the Barone group,[13] the values for peaks in the experimental vibrational spectrum from the ground state, and the results of our MM calculations. Note that the MM listings give the frequency for which the coefficient of the fundamental is largest. In many cases, the fundamental and its intensity are split between several of the CI states.

The DFT results for the global minimum shown in the first column of Table 1 are quite consistent with the harmonic frequencies based on the global minimum of our PES (fourth column). The generalized second-order Vibrational Perturbation Theory (GVPT2) results[13] in the second column are in much better agreement with the experimental ones than either the DFT results or the harmonic frequencies from our PES. Our MM results are generally in better agreement with experiment than the PES harmonic frequencies, but they are not as good at predicting experiment as the GVPT2 results. The mean absolute error (MAE), as compared to experiment, is 7.8 $cm^{-1}$ for the GVPT2 results and 36.2 $cm^{-1}$ for the MM ones. However, MM with this PES is still quite reasonable, and, as a global surface, the PES can be used to examine many kinetic properties, one of which will be discussed below.

Results for absorption from Conformer II, shown in Table 2, are similar in nature to those for absorption from the global minimum. The DFT and harmonic potential energy surface vibrational levels are again in good agreement with one another. As compared to

experiment, the MAE for the GVPT2 results is 11.3 $cm^{-1}$ and 36 $cm^{-1}$ for the MM.

**Table 1: Comparison of vibrational energies for the vibrational spectrum starting from the glycine global minimum (Conformer I). All energies are in $cm^{-1}$ relative to the ZPE.**

| DFT[a] | GVPT2[b] | Expt[c] | PES-HO[d] | MM CI[e] |
|---|---|---|---|---|
| 65 | – | – | 63 | 153 |
| 245 | 203 | 204 | 212 | 297 |
| 310 | 255 | 250 | 258 | 345 |
| 509 | 461 | 458 | 460 | 495 |
| 548 | 494 | 500 | 506 | 545 |
| 644 | 633 | 615 | 632 | 661 |
| 817 | 603 | 619 | 654 | 701 |
| 864 | 802 | 801 | 819 | 823 |
| 890 | 863 | 883 | 911 | 902 |
| 922 | 907 | 907 | 918 | 945 |
| 1068 | 1103 | 1101 | 1126 | 1132 |
| 1165 | 1144 | 1136 | 1162 | 1169 |
| 1214 | 1164 | 1166 | 1184 | 1193 |
| 1332 | 1286 | 1297 | 1306 | 1297 |
| 1352 | 1353 | 1340 | 1373 | 1384 |
| 1415 | 1387 | 1405 | 1389 | 1386 |
| 1461 | 1435 | 1429 | 1431 | 1446 |
| 1659 | 1612 | 1608 | 1676 | 1625 |
| 1846 | 1774 | 1779 | 1806 | 1802 |
| 3062 | 2947 | 2943 | 3046 | 2971 |
| 3108 | 2961 | 2969 | 3088 | 2985 |
| 3463 | 3367 | 3359 | 3498 | 3409 |
| 3533 | 3418 | 3410 | 3565 | 3453 |
| 3614 | 3575 | 3585 | 3729 | 3594 |

[a]ref. 13, Table 4
[b]ref. 13, Table 8
[c]experiment, as cited in ref. 13, Table 8
[d]harmonic frequencies determined by MULTIMODE for the glycine PES.
[e]from MULTIMODE calculation – frequency whose coefficient for the fundamental is highest.

**Table 2: Comparison of vibrational energies for the vibrational spectrum starting from the minimum of glycine Conformer II. All energies are in $cm^{-1}$ relative to the ZPE.**

| DFT[a] | GVPT2[b] | Expt[c] | PES-HO[d] | MM CI[e] |
|---|---|---|---|---|
| 40 | | | 57 | 154 |
| 245 | 232 | | 247 | 334 |
| 310 | 304 | 303 | 305 | 366 |
| 509 | 506 | | 508 | 534 |
| 548 | 543 | | 546 | 580 |
| 644 | 638 | | 638 | 666 |
| 817 | 784 | 786 | 812 | 815 |
| 864 | 785 | 808 | 853 | 861 |
| 890 | 851 | 867 | 885 | 890 |
| 922 | 896 | 911 | 925 | 940 |
| 1068 | 1061 | 1059 | 1067 | 1068 |
| 1165 | 1158 | | 1159 | 1170 |
| 1224 | 1182 | 1189 | 1211 | 1201 |
| 1332 | 1312 | | 1322 | 1323 |
| 1352 | 1325 | | 1352 | 1339 |
| 1415 | 1364 | 1390 | 1422 | 1396 |
| 1461 | 1432 | | 1448 | 1450 |
| 1659 | 1599 | 1622 | 1659 | 1597 |
| 1846 | 1793 | 1790 | 1828 | 1840 |
| 3062 | 2956 | 2941 | 3058 | 3006 |
| 3108 | 2976 | 2968 | 3106 | 3013 |
| 3463 | 3294 | 3275 | 3463 | 3228 |
| 3533 | 3384 | 3381 | 3526 | 3444 |
| 3614 | 3454 | 3447 | 3608 | 3467 |

[a]ref. 13, Table 4
[b]ref. 13, Table 8
[c]experiment, as cited in ref. 13, Table 8
[d]harmonic frequencies determined by MULTIMODE for the glycine PES.
[e]from MULTIMODE calculation – frequency whose coefficient for the fundamental is highest.

## MULTIMODE Spectra

To begin we show cuts of the new dipole moment vs normal mode for the indicated mode and conformer in Figure 1. In MULTIMODE, the $x$, $y$, and $z$ axes correspond to three principal axes B, C, A, respectively. As can be seen in the figure, the cuts of the dipole moment are quite nonlinear as a function of $Q$. Therefore, using a linear dipole, e.g., the double harmonic approximation, may be inaccurate for the IR intensities.

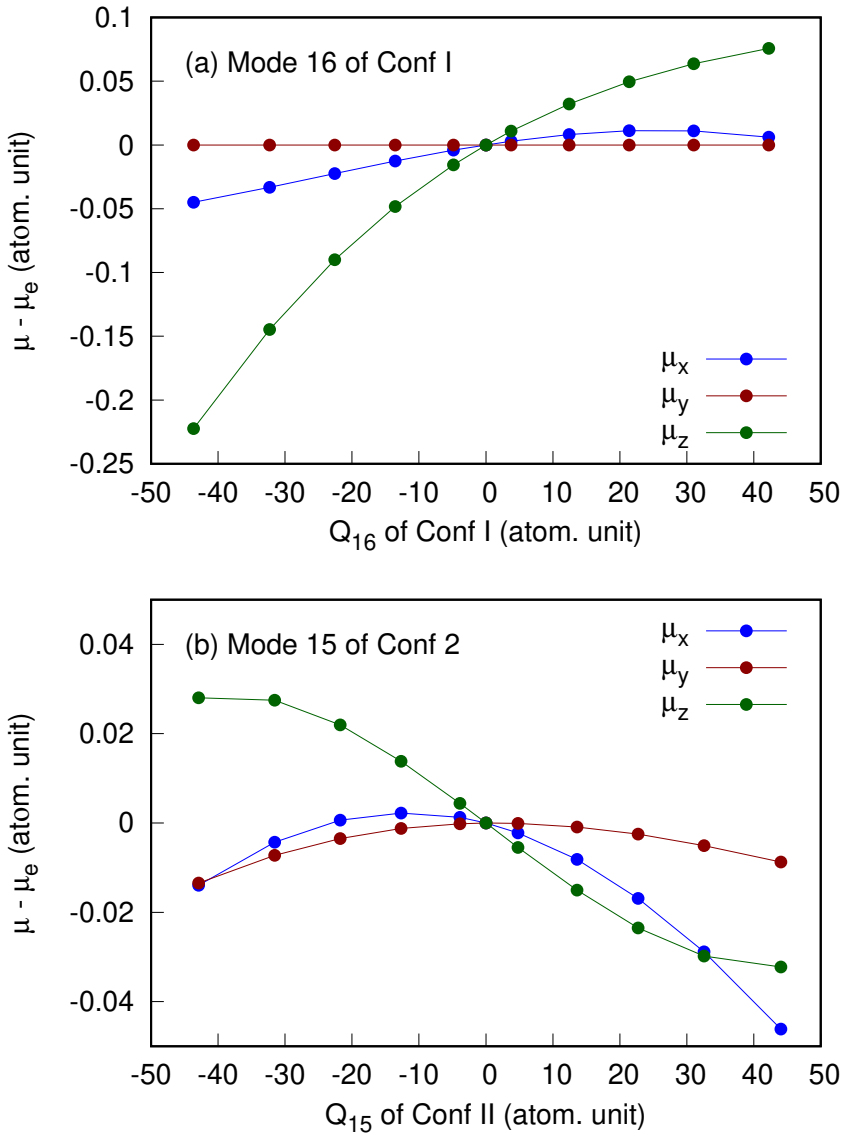


Figure 1: Dipole moment versus indicated normal mode for indicate confomer

Figure 2 shows a comparison between the experimental spectrum of Stepanian et al.,[9] the

spectrum calculated by the Barone group using GVPT2, and that for transitions from the ground state calculated using MM and our potential energy surface. In order to emphasize the relative intensities, we have used two adjustable amplitude parameters to compare the two calculated spectra with the experimental spectrum. There is good agreement between the three spectra on the intensities of most of the peaks, but the MM ones appear to be shifted somewhat to higher energy than the experimental ones. The GVPT2 ones are a bit closer in energy to the experimental ones than the MM peaks. Nonetheless, the general agreement between all three spectra is good. Note that the experimental peak at 3200 $cm^{-1}$ has been shown to be due to the presence of small concentrations of Conformer II.[22]

Figure 3 shows a comparison between the experimental peaks,[26] the GVPT2 calculations,[13] and the MM results for the spectra starting from Conformer II. Again, there are two arbitrary adjustable parameters for setting the intensities. The general agreement is excellent, showing that the GVPT2 and MM calculations are performing well. Of particular interest is the fact that both the GVPT2 and MM calculations produce a peak near 3200 $cm^{-1}$, known to be attributable to absorption from Conformer II.[22] The MM peak is reasonably broad due to substantial mixing of levels, but its breadth is comparable to the experimental peaks shown in Fig. 3B, peak h of ref. 26 or Fig. 2b of ref. 22.

## Tunneling

In 2012, Bazsó et al.[22] reported an interesting experiment in which Conformer I of glycine was excited by a pulsed, mid-IR laser on the overtone of its OH stretch. It was observed that this excitation depleted population from Conformer I and created population in Conformer VI. Subsequently, even in the dark, Conformer VI decayed to Conformer I so that the original spectrum was recovered after a measurable time period. Noting that the two Conformers I and VI are related by a 180° rotation of the OH hydrogen around the C-O axis, the thesis of the experimental interpretation was that the transformation involved tunneling of the hydrogen through a torsional barrier from Conformer VI to Conformer I. Deuteration at the

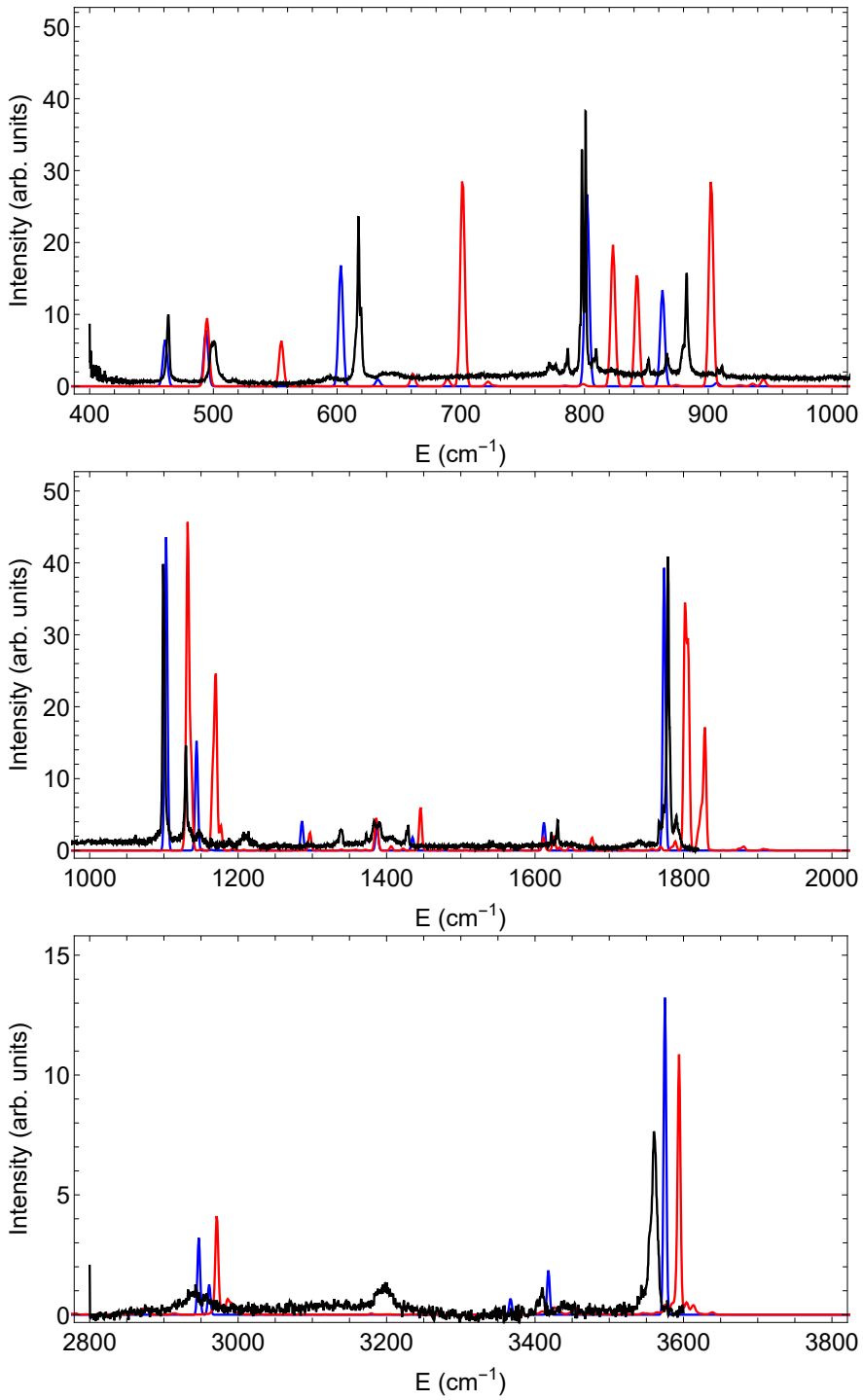


Figure 2: Comparison of experimental spectrum[9] (black) and GVPT2 (blue) results[13] with the ground state spectrum calculated using MULTIMODE and the glycine PES (red). The calculated spectra assume a FWHM linewidth of 5 cm$^{-1}$. The experimental peak at 3200 cm$^{-1}$ is due to a small amount of Conformer II.

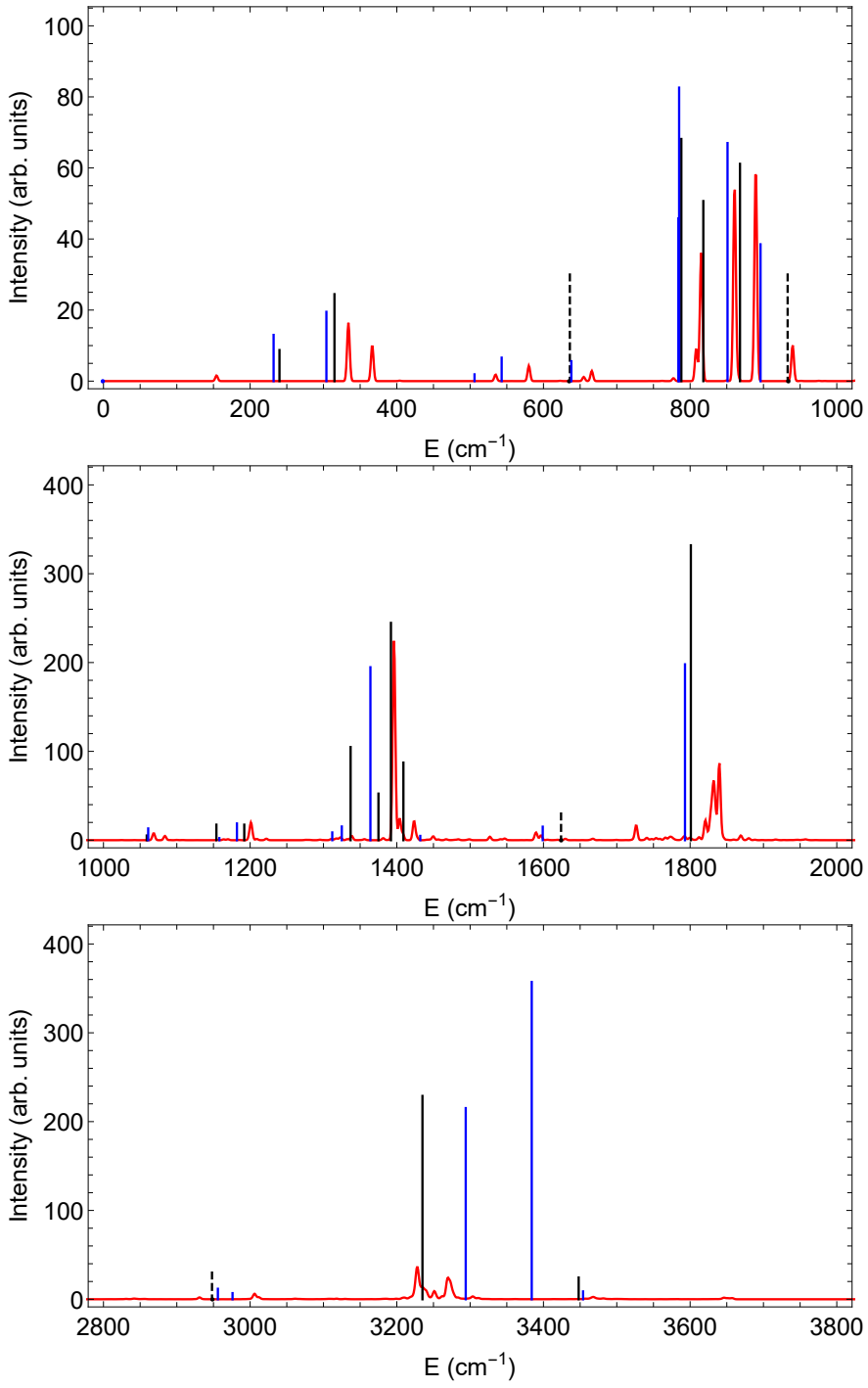


Figure 3: Comparison of experimental stick spectrum[26] (black) and GVPT2 (blue) stick spectrum[13] with the Conformer II spectrum calculated using MULTIMODE and the glycine PES (red). The MULTIMODE spectrum is plotted with a FWHM linewidth of 5 cm$^{-1}$. The dashed black lines represent peaks in the spectrum for which the intensity is not reported.

hydrogen site resulted in lowering the rate of recovery by many orders of magnitude.

We have calculated tunneling in glycine using our glycine PES in order to test the thesis that tunneling is responsible for the experimental observation and to investigate whether a simple model might be useful. As mentioned, the path by which Conformer VI is transformed into Conformer I is principally the rotation of the OH group around the CO bond. Previous successful one-dimensional estimates[58,60,61] have used a $Q_{im}$ path that follows the imaginary frequency barrier between the two conformers. In these examples, the normal mode vector at the saddle point indicates motion that will lead very closely to one of the two conformers. While this $Q_{im}$ path is effective for many problems, in a torsional coordinate the normal mode vector at the saddle point is tangent to the circular path and thus will point far away from either conformer; what we really want is an arcing torsional path. A simple analysis shows that the $Q_{im}$ path underestimates the path length for integration by about a factor of $\pi/2$ and thus gives much too small a half-life. Indeed, using the $Q_{im}$ path for the Conformer VI to Conformer I tunneling transition underestimates the tunneling half-life in glycine by six orders of magnitude. The torsional path does much better.

As a first step to examine the torsional path, we calculated the potential energy of glycine at each point along the semi-circular torsional path at points separated by a change in angle of 0.5°, assuming that all other coordinates were fixed at their original values for Conformer VI. The potential energy for this "unrelaxed" path is similar to that shown in Fig. 4 except that it is a bit longer and has slightly higher barriers. The potential shown in the figure is for a "relaxed" path, where all coordinates are allowed to take whatever values minimize the energy at each rotational angle. The principal change is in the distance $r$ of the rotating H atom from the CO axis; it changes from 0.90 Å at Conformer VI, to 0.88 Å at the transition state and 0.92 Å at Conformer I.

The ZPE for Conformer VI was found to be 227 $cm^{-1}$ using the DVR technique (which also gave the other energy levels shown in the figure). Then in Eq. 4, $\omega/2\pi = \nu = 2(227)c$, where $c$ is the speed of light. The integral in Eq. 5 was performed numerically with $E=$

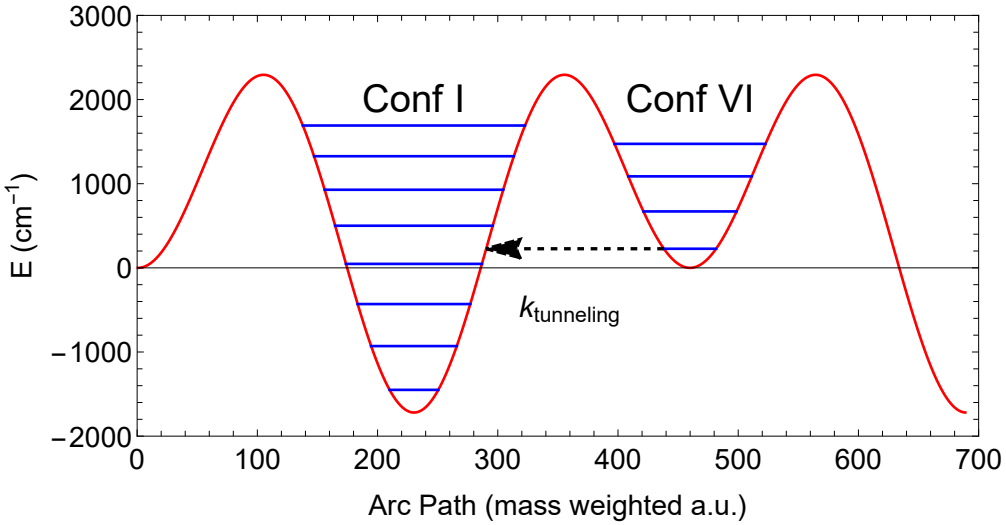


Figure 4: Tunneling from Conformer VI to Conformer I along a rotational path arc of the OH group around the CO bond, where the potential energy of all other modes is relaxed. The zero point energy of Conformer VI is 227 cm$^{-1}$.

227 cm$^{-1}$ and the potential $V(Q)$ shown in Fig. 4. Using the rate constant obtained from Eq. 4, we found the half-life of Conformer VI to be 0.43 s. The experimental result depends somewhat on the nature of the matrix, but it ranges from 2.8 to 4.4 s. For the triply deuterated glycine (with two D atoms bonded to the N and one to the O), the calculated half-life is 202 hours whereas the experimental result is 48 to 99.3 hours. Despite the fact that the calculated values are not in perfect agreement with the experimental results, one should note that an uncertainty of ±10% in the value of the integral leads to a value of the half-life that is divided or multiplied by a factor of nearly 20. The path for integration that we have used is a fairly simple one, so that the integral could easily be over- or under-estimated by 10%. Thus, the near agreement means that the surface is probably not too far off from one that would agree more accurately with experiment.

One further improvement was considered. We calculated the energies of the two conformers and the transition state using coupled cluster single-double and perturbative triple excitations, CCSD(T), with Dunning's aug-cc-pVDZ basis set. Although the saddle point did not fully converge, we took the lowest energy obtained. In the DFT calculation the saddle point referenced to the global minimum (Conformer I) was 4010.7 cm$^{-1}$ and 2292.3

$cm^{-1}$ when referenced to Conformer VI. In the CCSD(T) results the similar numbers were 4148.2 $cm^{-1}$ and 2500.7 $cm^{-1}$. Thus, the barrier to tunneling would be about 200 $cm^{-1}$ higher for a CCSD(T) surface, lengthening the half-life somewhat for both the H and D versions of glycine. A simple "morphed" version of the relaxed potential, adjusted to give a barrier of 2500 $cm^{-1}$ consistent with the CCSD(T) calculation, resulted in a half-life of 7 s. Information about the CCSD(T) results for Conformers I, II, III and VI, including geometries, energies, and harmonic frequencies, is provided in the Supplementary Information (SI).

## Comments about a sGDML glycine potential

At about the same time we reported our PIP glycine potential,[2] a potential from the Tkatchenko group was reported.[5] Their PES was a fit to DFT/PBE gradients using the sGDML method developed by that group and was limited to describing the isomerization of conformer I to conformer III. The aim of that work is expressed directly by the title "Challenges for machine learning force fields in reproducing potential energy surfaces of flexible molecules". The methods considered were sGDML, SchNet, Gaussian Approximation Potentials/Smooth Overlap of Atomic Positions (GAPs/SOAPs), and Behler-Parrinello neural networks (BP-NN). The latter two are well-known atom-centered ML methods. The conclusion was that all the methods examined have issues with their descriptors, with the BP-NN method performing the worst and the sGDML performing the best.

A detailed discussion of the reviewed approaches[5] and a comparison to the PIP one[2] is certainly worthwhile for the future. Here we simply note that we obtained the sGDML PES from the Tkatchenko group and have used it in standard optimizations of the two minima followed by normal mode analyses. The results are given in the SI. Briefly, the mean absolute errors, as compared to the benchmark CCSD(T) calculations, were 9.9 $cm^{-1}$ for our PIP surface and 36.9 $cm^{-1}$ for the sGDML surface for Conformer I and 14.5 $cm^{-1}$ for the PIP surface and 43.4 $cm^{-1}$ for the sGDML surface for Conformer III. These differences

were, to some extent, due to the different DFT functionals used, B3LYP in our case and PBE in the sGDML case.

The sGDML surface was based on a data set of 5000 energies and associated gradients obtained using *ab initio* molecular dynamics calculations at temperature of 500 K. The energy distributions for the PIP and sGDML surfaces are given in Fig. S1 of the SI. The sGDML distribution has a peak just above 4000 $cm^{-1}$, which is less than one quarter of the zero-point energy (17 205 $cm^{-1}$). Thus, the molecular dynamics calculations explored only a fraction of the configuration space corresponding to the zero point motions. Of course, it was never intended that the sGDML surface would be accurate except for the path between Conformers I and III, nor was it the intention for the SGDML surface to be used for dynamics. On the sGDML PES, conformer III is 563 $cm^{-1}$ higher, and the barrier height of the I $\rightarrow$ III isomerization is 678 $cm^{-1}$. The numbers from our PIP PES are 577 $cm^{-1}$ and 778 $cm^{-1}$, respectively. The differences between these values were primarily due to the different DFT functionals used.

However, it is clear that the sGDML PES is limited with respect to coverage of total energies and description of conformers compared to the PIP one. In fact, the sGDML PES has many holes even at relatively low energies for these conformers and, as expected, it produces unphysical results for other conformers. We do note our PES was refined numerous times to eliminate holes that we discovered in extensive diffusion Monte Carlo calculations for each conformer. Without doubt, our PES still has holes at very high energies and for configurations that describe any feasible fragmentation channel. Holes are an inevitable feature of a machine-learned potential and so we might offer the following dictum "If the PES has holes it was probably machine learned".

# Conclusions

The PES for glycine[2] has been used to determine the infrared spectrum for absorption both from Conformer I and from Conformer II. Quite reasonable agreement with the fundamental frequencies has been found with previous results, as shown in Tables 1 and 2. In addition, the comparison with the experimental spectra is also quite good, as shown in Figures 2 and 3. The PES has also been used to investigate tunneling from Conformer VI to Conformer I. The experimental result for the tunneling half-life for H is 2.8–4.4 s, depending on the nature of the matrix used to isolate the glycine.[22] Analysis along a 1d torsional tunneling path of the PES, allowing for relaxation of all other coordinates, gives a half-life of 0.43 s for the DFT-based PES and 7 s for a surface modified so as to have a barrier in agreement with CCSD(T) calculations. Both experiment and calculation show that the tunneling rate for D is orders of magnitude slower, on the order of 50–200 hours. In general both spectroscopic and kinetic calculations show that an improvement in the description of the electronic structure beyond the DFT level is helpful in achieving better results. We have recently developed a $\Delta$ machine learning approach to make that feasible.[62]

Another possible use for the full-dimensional glycine PES might be in calibrating machine learning (ML) techniques for prediction of dynamics in glycine as well as in larger, similarly flexible molecules. For example, the Tkatchenko group has recently considered several ML models as applied both to the isomerization in glycine between Conformers I and II and to the *cis* to *trans* relaxation in azobenzene.[5] Accurate potential energy surfaces, tested against experimental spectra and dynamical measurements of tunneling and isomerization rates will be particularly useful. In this regard the dataset used for the glycine PIP PES is available at https://scholarblogs.emory.edu/bowman/potential-energy-surfaces/

## Acknowledgement

JMB thanks the Army Research Office, DURIP grant (W911NF-14-1-0471), for funding a computer cluster where most of the calculations were performed. We thank Prof. Alexandre Tkatchenko and Valentin Vassilev Galindo for sending the glycine sGDML PES. JMB thanks Alexandre Tkatchenko for discussions.

## Supporting Information Available

Tables providing information on the results of CCSD(T)/aug-cc-pVDZ results on the optimized structure energies, geometries as well as and harmonic vibrational energies for Conformers I, II, III, and VI, with comparison to B3LYP/aug-cc-pVDZ, PIP-PES surface, and sGDML surface frequencies.[5] Figures showing the histograms of energies in the data sets for our PIP PES and for the sGDML one.

# TOC Figure

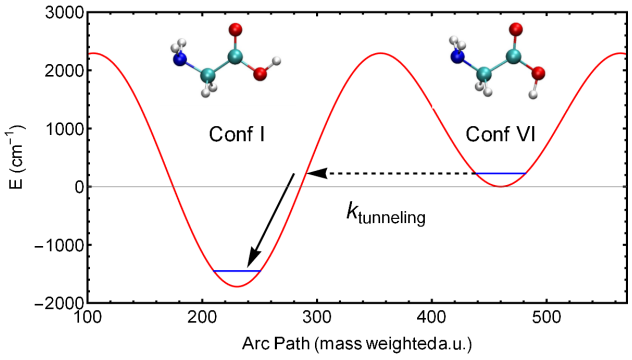


# References


(1) Barone, V.; Biczysko, M.; Bloino, J.; Puzzarini, C. Characterization of the Elusive Conformers of Glycine from State-of-the-Art Structural, Thermodynamic, and Spectroscopic Computations: Theory Complements Experiment. *J. Chem. Theory Comput.* **2013**, *9*, 1533–1547.

(2) Conte, R.; Houston, P. L.; Qu, C.; Li, J.; Bowman, J. M. Full-dimensional, ab Initio Potential Energy Surface for Glycine with Characterization of Stationary Points and Zero-point Energy Calculations by Means of Diffusion Monte Carlo and Semiclassical Dynamics. *J. Chem. Phys.* **2020**, *153*, 244301:1–11.

(3) Császár, A. G. Conformers of Gaseous Glycine. *J. Am. Chem. Soc.* **1992**, *114*, 9568–9575.

(4) Orjan, E. M.; Nacsa, A. B.; Czakó, G. Conformers of Dehydrogenated Glycine Insomers. *J. Comput. Chem.* **2020**, *41*, 2001–2014.

(5) Vassilev-Galindo, B.; Fonseca, G.; Poltavsky, I.; Tkatchenko, A. Challenges for Machine Learning Force Fields in Reproducing Potential Energy Surfaces of Flexible Molecules. *J. Chem. Phys.* **2021**, *154*, 094119:1–14.

(6) Behler, J. Neural Network Potential-Energy Surfaces in Chemistry: a Tool for Large-scale Simulations. *Phys. Chem. Chem. Phys.* **2011**, *13*, 17930–17955.

(7) Schütt, K. T.; Sauceda, H. E.; Kindermans, P.-J.; Tkatchenko, A.; Müller, K.-R. SchNet - A Deep Learning Architecture for Molecules and Materials. *J. Chem. Phys.* **2018**, *148*, 241722:1–11.

(8) Bartók, A. P.; Payne, M. C.; Kondor, R.; Csányi, G. Gaussian Approximation Potentials: The Accuracy of Quantum Mechanics, without the Electrons. *Phys. Rev. Lett.* **2010**, *104*, 136403:1–4.

(9) Stepanian, S. G.; Reva, I. D.; Radchenko, E. D.; Rosado, M. T. S.; Duarte, M. L. T. S.; Fausto, R.; Adamowicz, L. Matrix-Isolation Infrared and Theoretical Studies of the Glycine Conformers. *J. Phys. Chem. A* **1998**, *102*, 1041–1054.

(10) Brauer, B.; Chaban, G. M.; Gerber, R. B. Spectroscopically-tested, Improved, Semi-empirical Potentials for Biological Molecules: Calculations for Glycine, Alanine and Proline. *Phys. Chem. Chem. Phys.* **2004**, *6*, 2543–2556.

(11) Senent, M.; Villa, M.; Dominguez-Gomez, R.; Fernandez-Clavero, A. Ab Initio Study of the Far Infrared Spectrum of Glycine. *Int. J. Quantum Chem.* **2020**, *104*, 551–561.

(12) Bludsky, O.; Chocholousova, J.; Vacek, J.; Huisken, F.; Hobza, P. Anharmonic Treatment of the Lowest-energy Conformers of Glycine: A Theoretical Study. *J. Chem. Phys.* **2000**, *113*, 4629–4635.

(13) Barone, V.; Biczysko, M.; Bloino, J.; Puzzarini, C. Accurate Structure, Thermodynamic and Spectroscopic Parameters from CC and CC/DFT Schemes: the Challenge of the Conformational Equilibrium in Glycine. *Phys. Chem. Chem. Phys.* **2013**, *15*, 10094–10111.

(14) Gabas, F.; Conte, R.; Ceotto, M. On-the-Fly ab Initio Semiclassical Calculation of Glycine Vibrational Spectrum. *J. Chem. Theory Comput.* **2017**, *13*, 2378–2388.

(15) Bloino, J.; Barone, V. A Second-order Perturbation Theory Route to Vibrational Averages and Transition Properties of Molecules: General Formulation and Application to Infrared and Vibrational Circular Dichroism Spectroscopies. *J. Chem. Phys.* **2012**, *136*, 124108:1–15.

(16) Biczysko, M.; Bloino, J.; Carnimeo, I.; Panek, P.; Barone, V. Fully ab Initio IR Spectra for Complex Molecular Systems from Perturbative Vibrational Approaches: Glycine as a Test Case. *J. Mol. Spect.* **2012**, *1009*, 74–82.

(17) Micciarelli, M.; Gabas, F.; Conte, R.; Ceotto, M. An Effective Semiclassical Approach to IR Spectroscopy. *J. Chem. Phys.* **2019**, *150*, 184113:1–12.

(18) Kuan, Y.-J.; Charnley, S. B.; Huang, H.-C.; Tseng, W.-L.; Kisiel, Z. Interstellar Glycine. *Astrophys. J.* **2003**, *593*, 848–867.

(19) Snyder, L. E.; Lovas, F. J.; Hollis, J. M.; Friedel, D. N.; Jewell, P. R.; Raemijan, A.; Ilyushin, V. V.; Alekseev, E. A.; Dyubko, S. F. A Rigorous Attempt to Verify Interstellar Glycine. *Astrophys. J.* **2005**, *619*, 914–930.

(20) Jones, P. A.; Cunningham, M. R.; Godfrey, P. D.; Cragg, D. M. A Search for Biomolecules in Sagittarius B2 (LMH) with the Australia Telescope Compact Array. *Mon. Not. R. Astron. Soc.* **2007**, *374*, 579–589.

(21) Cunningham, M. R.; Jones, P. A.; Godfrey, P. D.; Cragg, D. M.; Bains, I.; Burton, M. G.; Calisse, P.; Crighton, N. J. M.; Curran, S. J.; Davis, T. M. et al. A Search for Propylene Oxide and Glycine in Sagittarius B2 (LMH) and Orion. *Mon. Not. R. Astron. Soc.* **2007**, *376*, 1201–1210.

(22) Bazsó, G.; Magyarfalvi, G.; Tarczay, G. Near-infrared Laser Induced Conformational Change and UV laser Photolysis of Glycine in Low-temperature Matrices: Observation of a Short-lived Conformer. *J. Mol. Struct.* **2012**, *1025*, 33–42.

(23) Bazsó, G.; Magyarfalvi, G.; Tarczay, G. Tunneling Lifetime of the ttc/VIp Conformer of Glycine in Low-Temperature Matrices. *J. Phys. Chem. A* **2012**, *116*, 10539–10547.

(24) Coussan, S.; Tarczay, G. Infrared Laser Induced Conformational and Structural Changes of Glycine and Glycine·Water Complex in Low-temperature Matrices. *Chem. Phys. Lett.* **2016**, *644*, 189–194.

(25) Huisken, F.; Werhahn, O.; Ivanov, A. Y.; Krasnokutski, S. A. The O-H stretching Vibrations of Glycine Trapped in Rare Gas Matrices and Helium Clusters. *J. Chem. Phys.* **1999**, *111*, 2978–2984.

(26) Ivanov, A. Y.; Sheina, G.; Blagoi, Y. P. FTIR Spectroscopic Study of the UV-induced Rotamerization of Glycine in the Low Temperature Matrices (Kr, Ar, Ne). *Spectrochim. Acta* **1999**, *55*, 219–228.

(27) Kumar, S. .; Rai, A. R.; Singh, V. B.; Rai, S. B. Vibrational Spectrum of Glycine Molecule. *Spectrochim. Acta* **2005**, *61*, 2741–2746.

(28) Balabin, R. M. Conformational Equilibrium in Glycine: Experimental Jet-Cooled Raman Spectrum. *J. Phys. Chem. Lett.* **2010**, *1*, 20–23.

(29) Balabin, R. M. Experimental Thermodynamics of Free Glycine Conformations: the First Raman Experiment after Twenty Years of Calculations. *Phys. Chem. Chem. Phys.* **2012**, *14*, 99–103.

(30) Bowman, J. M. Self-consistent Field Energies and Wavefunctions for Coupled Oscillators. *J. Chem. Phys.* **1978**, *68*, 608–610.

(31) Carter, S.; Culik, S. J.; Bowman, J. M. Vibrational Self-consistent Field method for Many-mode Systems: A New Approach and Application to the Vibrations of CO Adsorbed on Cu(100). *J. Chem. Phys.* **1997**, *107*, 10458–10469.

(32) Bowman, J. M.; Carter, S.; Huang, X. MULTIMODE: a Code to Calculate Rovibrational Energies of Polyatomic Molecules. *Int. Rev. Phys. Chem.* **2003**, *22*, 533–549.

(33) Bowman, J. M. The Self-consistent-field Approach to Polyatomic Vibrations. *Acc. Chem. Res.* **1986**, *19*, 202–208.

(34) Christoffel, K.; Bowman, J. Investigations of Self-consistent Field, SCF CI and Virtual state Configuration Interaction Vibrational Energies for a Model Three-mode System. *Chem. Phys. Lett.* **1982**, *85*, 220–224.

(35) Carter, S.; Bowman, J. M.; Handy, N. C. Extensions and Tests of "Multimode": A Code to Obtain Accurate Vibration/Rotation Energies of Many-Mode Molecules. *Theor. Chem. Acc.* **1998**, *100*, 191–198.

(36) Watson, J. K. G. Simplification of the Molecular Vibration-Rotation Hamiltonian. *Mol. Phys.* **1968**, *15*, 479–490.

(37) Ostrowski, L.; Ziegler, B.; Rauhut, G. Tensor Decomposition in Potential Energy Surface Representations. *J. Chem. Phys.* **2016**, *145*, 104103:1–9.

(38) Ziegler, B.; Rauhut, G. Efficient Generation of Sum-of-products Representations of High-dimensional Potential Energy Surfaces Based on Multimode Expansions. *J. Chem. Phys.* **2016**, *144*, 114114:1–11.

(39) Christiansen, O. Selected New Developments in Vibrational Structure Theory: Potential Construction and Vibrational Wave Function Calculations. *Phys. Chem. Chem. Phys.* **2012**, *14*, 6672–6687.

(40) König, C.; Christiansen, O. Automatic Determination of Important Mode-mode Correlations in Many-mode Vibrational Wave Functions. *J. Chem. Phys.* **2015**, *142*, 144115:1–19.

(41) Schröder, B.; Rauhut, G. Incremental Vibrational Configuration Interaction Theory, iVCI: Implementation and Benchmark Calculations. *J. Chem. Phys.* **2021**, *154*, 124114:1–12.

(42) Dinu, D. F.; Ziegler, B.; Podewitz, M.; Liedl, K. R.; Loerting, T.; Grothe, H.; Rauhut, G. The Interplay of VSCF/VCI Calculations and Matrix-isolation IR Spectroscopy - Mid Infrared Spectrum of $CH_3CH_2F$ and $CD_3CD_2F$. *J. Mol. Spectrosc.* **2020**, *367*, 111224:1–11.

(43) Erfort, S.; Tschöpe, M.; Rauhut, G. Toward a Fully Automated Calculation of Rovibrational Infrared Intensities for Semi-rigid Polyatomic Molecules. *J. Chem. Phys.* **2020**, *152*, 244104:1–14.

(44) Schmitz, G.; Artiukhin, D. G.; Christiansen, O. Approximate High Mode Coupling Potentials Using Gaussian Process Regression and Adaptive Density Guided Sampling. *J. Chem. Phys.* **2019**, *150*, 131102:1–7.

(45) Madsen, N. K.; Jensen, R. B.; Christiansen, O. Calculating Vibrational Excitation Energies Using Tensor-decomposed Vibrational Coupled-cluster Response Theory. *J. Chem. Phys.* **2021**, *154*, 054113:1–14.

(46) Moitra, T.; Madsen, D.; Christiansen, O.; Coriani, S. Vibrationally Resolved Coupled-cluster X-ray Absorption Spectra From Vibrational Configuration Interaction Anharmonic Calculations. *J. Chem. Phys.* **2020**, *153*, 234111:1–18.

(47) Bowman, J. M.; Carrington, T.; Meyer, H.-D. Variational Quantum Approaches for Computing Vibrational Energies of Polyatomic Molecules. *Mol. Phys.* **2008**, *106*, 2145–2182.

(48) Carter, S.; Bowman, J. M.; Handy, N. C. Multimode calculations of Rovibrational Energies of $C_2H_4$ and $C_2D_4$. *Mol. Phys.* **2012**, *110*, 775–781.

(49) Carter, S.; Sharma, A. R.; Bowman, J. M. First-principles Calculations of Rovibrational Energies, Dipole Transition Intensities and Partition Function for Ethylene Using MULTIMODE. *J. Chem. Phys.* **2012**, *137*, 154301:1–19.

(50) Roy, T. K.; Gerber, R. B. Vibrational Self-consistent Field Calculations for Spectroscopy of Biological Molecules: New Algorithmic Developments and Applications. *Phys. Chem. Chem. Phys.* **2013**, *15*, 9468–9492.

(51) Oschetzki, D.; Rauhut, G. Pushing the Limits in Accurate Vibrational Structure Calculations: Anharmonic Frequencies of Lithium Fluoride Clusters (LiF)n, n = 2—10. *Phys. Chem. Chem. Phys.* **2014**, *16*, 16426–16435.

(52) Császár, A. G.; Fabri, C.; Szidarovszky, T.; Matyus, E.; Furtenbacher, T.; Czakó, G. The Fourth Age of Quantum Chemistry: Molecules in Motion. *Phys. Chem. Chem. Phys.* **2012**, *14*, 1085–1106.

(53) Tennyson, J. Perspective: Accurate Ro-vibrational Calculations on Small Molecules. *J. Chem. Phys.* **2016**, *145*, 120901:1–8.

(54) Wang, X.; Carter, S.; Bowman, J. M. Pruning the Hamiltonian Matrix in MULTIMODE: Test for $C_2H_4$ and Application to $CH_3NO_2$ Using a New ab Initio Potential Energy Surface. *J. Phys. Chem. A* **2015**, *119*, 11632–11640.

(55) Carrington, T. Perspective: Computing (Ro-)vibrational Spectra of Molecules with More than Four Atoms. *J. Chem. Phys.* **2017**, *146*, 120902:1–10.

(56) Werner, H.-J.; Knowles, P. J.; Manby, F. R.; Black, J. A.; Doll, K.; Heßelmann, A.; Kats, D.; Köhn, A.; Korona, T.; Kreplin, D. A. et al. The Molpro Quantum Chemistry Package. *J. Chem. Phys.* **2020**, *152*, 144107:1–24.

(57) Bowman, J. M.; Huang, X.; Handy, N. C.; Carter, S. Vibrational Levels of Methanol Calculated by the Reaction Path Version of MULTIMODE, Using an ab Initio, Full-Dimensional Potential. *J. Phys. Chem. A* **2007**, *111*, 7317–7321.

(58) Wang, Y.; Bowman, J. M. Bend Excitation Is Predicted to Greatly Accelerate Isomerization of trans-Hydroxymethylene to Formaldehyde in the Deep Tunneling Region. *J. Phys. Chem. Lett.* **2015**, *6*, 124–128.

(59) Colbert, D. T.; Miller, W. H. Large-amplitude Dynamics in Vinyl Radical: The Role of Quantum Tunneling as an Isomerization Mechanism. *J. Chem. Phys.* **1992**, *96*, 1982–1991.

(60) Wang, Y.; Bowman, J. M. One-dimensional Tunneling Calculations in the Imaginary-frequency, Rectilinear Saddle-point Normal Mode. *J. Chem. Phys.* **2008**, *129*, 121103:1–5.

(61) Wang, Y.; Bowman, J. M. Mode-specific Tunneling Using the Qim Path: Theory and an Application to Full-dimensional Malonaldehyde. *J. Chem. Phys.* **2013**, *139*, 154303:1–5.

(62) Nandi, A.; Qu, C.; Houston, P. L.; Conte, R.; Bowman, J. M. $\Delta$-machine Learning for Potential Energy Surfaces: A PIP Approach to Bring a DFT-based PES to CCSD(T) Level of Theory. *J. Chem. Phys.* **2021**, *154*, 051102:1–8.